Journal of
Applied Remote Sensing

RemoteSensing.SPIEDigitalLibrary.org

Passive CubeSats for remote inspection of space vehicles

Patrick Walton
Josh Cannon
Brian Damitz
Tyler Downs
Dallon Glick
Jacob Holtom
Nicholas Kohls
Alex Laraway
Iggy Matheson
Jason Redding
Cory Robinson
Jared Ryan
Niall Stoddard
Jacob Willis
Karl Warnick
Michael Wirthlin
Doran Wilde
Brian D. Iverson
David Long

Patrick Walton, Josh Cannon, Brian Damitz, Tyler Downs, Dallon Glick, Jacob Holtom, Nicholas Kohls, Alex Laraway, Iggy Matheson, Jason Redding, Cory Robinson, Jared Ryan, Niall Stoddard, Jacob Willis, Karl Warnick, Michael Wirthlin, Doran Wilde, Brian D. Iverson, David Long, "Passive CubeSats for remote inspection of space vehicles," *J. Appl. Remote Sens.* **13**(3), 032505 (2019), doi: 10.1117/1.JRS.13.032505.

SPIE.

Passive CubeSats for remote inspection of space vehicles

Patrick Walton,* Josh Cannon, Brian Damitz, Tyler Downs, Dallon Glick, Jacob Holtom, Nicholas Kohls, Alex Laraway, Iggy Matheson, Jason Redding, Cory Robinson, Jared Ryan, Niall Stoddard, Jacob Willis, Karl Warnick, Michael Wirthlin, Doran Wilde, Brian D. Iverson, and David Long

Brigham Young University, Department of Electrical and Computer Engineering, Provo, Utah, United States

Abstract. Remote inspection can supplement instrumentation to holistically characterize vehicle state, but for space vehicles in flight, inspection is often either risky or costly. We propose using passive inspection CubeSats (PICs) to reliably and affordably image the launch vehicle with fine resolution, moderate coverage, and rapid response. The PICs mission, developed by Brigham Young University undergraduate students and manifested for launch in 2019, is designed to demonstrate this approach using two redundant CubeSats. Each CubeSat uses a spherical array of six cameras, 12 light-emitting diode flash units, and a field-programmable gate array to rapidly boot after separation and capture spherical images of its entire surroundings, including the launch vehicle and other released CubeSats. The PIC bus system includes several custom components, including a compact 3500-mAh battery system, 1 to 2 W solar power system, chassis, omnidirectional antenna system, radio, and a small integrated remove-before-flight-pin and system access port. Preliminary test results suggest the PICs are able to boot within 1.1 s of separation and inspect 1-mm features on each other and their launch vehicle, regardless of the spin developed at separation. [DOI: 10.1117/1.JRS.13.032505]

Keywords: inspection; CubeSat; visual inspection; satellite servicing.

Paper 190239SS received Apr. 2, 2019; accepted for publication Jun. 19, 2019; published online Jul. 12, 2019.

1 Introduction

Remote inspection, which applies the tools of remote sensing to observe manmade systems, provides insight into the vehicle state that cannot be obtained by instrumentation alone. For space vehicles in flight, the complex dynamics of proximity operations makes the inspection challenging. Space vehicles that could benefit from inspection often lack the capability, either due to the cost or due to the risk of available inspectors.[1] We propose the use of passive inspection CubeSats (PICs) to reliably provide limited, low-cost inspection to space vehicles in flight. Brigham Young University (BYU) undergraduate students are developing the PICs mission to demonstrate the viability of using PICs to perform remote inspection of spacecraft.

The CubeSats are passive because they do not use maneuvering systems. This makes them safe to operate as they drift away from the upper stage of their launch vehicle. To perform inspection without pointing capabilities, PICs have a 360 deg × 180 deg (spherical) camera array, consisting of six wide-angle cameras, which provides visibility of the launch vehicle regardless of orientation. For this mission, two redundant demonstration units, PIC-A and PIC-B, are manifest on the 20th mission of the Educational Launch of Nanosatellites (ELaNa) program, operated by NASA Launch Services Program. The ELaNa-20 mission is expected to launch aboard Virgin Orbit's LauncherOne vehicle in 2019.

In this paper, we begin by describing prior approaches to remote inspection (Sec. 1.1) and our alternative approach, the PIC (Sec. 2). We describe the demonstration mission and the two

*Address all correspondence to Patrick Walton, E-mail: m.patrick.walton@gmail.com

1931-3195/2019/$28.00 © 2019 SPIE

identical CubeSats designed to demonstrate the PICs concept (Sec. 3). We conclude with our preliminary tests and the expected on-orbit performance (Sec. 4) of the PICs demonstration mission.

1.1 *Background*

In many vehicle domains, remote inspection provides a holistic complement to instrumentation for characterizing vehicle condition. Mission operations far from Earth make space vehicles difficult to inspect during flight. Existing approaches for remotely inspecting spacecraft involve ground-based instruments,[1] spacecraft rendezvous, astronaut extravehicular activity (EVA),[2] robotic arms,[3] on-board cameras,[4] and free-flying inspectors. Example results from these approaches are given in Fig. 1. We provide the motivation for PICs by discussing the trade-offs of these proven and proposed approaches. We then propose an alternative approach, using passive, free-flying CubeSats.

The various approaches to space vehicle inspection can be compared on several measures of performance, including net reliability, net affordability, coverage, spatial resolution, and response time. Net reliability can be expressed as $\Delta\rho_{\text{net}} = \Delta\rho_e - \Delta\rho_I$, where $\Delta\rho_e$ is the vehicle's expected reliability increase and $\Delta\rho_I$ is risk to the vehicle presented by the inspector. Net affordability can be expressed as $C_{\text{net}} = \Delta\rho_{\text{net}} C_V - C_I$, where C_V is the cost of the vehicle and C_I is the cost of inspection. Coverage, the degree to which the inspector can observe the entire exterior, is dependent on the mobility of the inspector and its target vehicle. Spatial resolution, which determines the smallest features resolvable by the inspector, depends on sensor resolution and

Fig. 1 Example results of prior approaches to remote inspection of space systems. (a) Foam impacting Space Shuttle Columbia 13's left wing during launch, imaged by ground-based cameras.[1] Public domain. Credit: NASA. (b) Space Shuttle Discovery 13's heat shields imaged by astronauts on ISS during a pitch maneuver on the first shuttle mission after the Columbia accident.[5] Public domain. Credit: NASA. (c) Wheel damage on Curiosity rover, imaged by the rover's MAHLI camera.[6] Public domain. Credit: NASA/JPL-Caltech/MSSS. (d) Space shuttle wing imaged by crew inside the orbiter.[1] Public domain. Credit: NASA.

Table 1 A qualitative comparison of the conventional approaches to spacecraft inspection.

Inspection method	Reliability	Affordability	Coverage	Resolution	Response time
Telescopes	**+**	**+**	**–**	**–**	**–**
Spacecraft rendezvous	**–**	**–**	**+**	**+**	**–**
EVA inspection	**–**	**–**	**+**	**+**	**–**
Dedicated robotic arm	**+**	**–**	**+**	**+**	**+**
General purpose arm	**+**	**+**	**–**	**–**	**+**
On-board inspection	**+**	**+**	**–**	**+**	**+**
Free-flying inspectors	**–**	**+**	**+**	**+**	**+**

Note: All the values are bold in order to improve readability.

distance. Response time depends primarily on initial proximity and setup time. Quantitative performance comparison is beyond the scope of this introduction, but a limited, qualitative comparison of conventional approaches motivates our alternative approach. The results of this qualitative evaluation, informed by our review of the relevant literature, are presented below as well as in Table 1.

To clearly describe and compare the various conventional approaches, we review each approach in the context of the Space Shuttle Columbia accident, which may be considered the seminal case study for the use of remote inspection as a complement to on-board instrumentation. During Columbia's 2003 launch, foam insulation broke from the external tank and struck the thermal protection system (TPS) on the leading edge of the left wing. Unable to determine the extent of the damage, program managers instructed the crew to reenter Earth's atmosphere, which resulted in loss of the vehicle and crew. The report of the accident investigation board determined that early, unequivocal confirmation of the "catastrophic damage … might have provided a window in which Atlantis could rendezvous with Columbia before Columbia's limited consumables ran out.[1]" Several approaches to inspection might have confirmed Columbia's condition but were not used or were unsuitable for impromptu application.

Telescopes may rapidly be tasked to inspect orbital vehicles with limited resolution at no risk and low cost; however, telescope response may be slow since the telescope must wait for the vehicle to come into its field of view. Vehicle roll maneuvers are required to enhance coverage since the telescope can only view the vehicle from one direction. Telescope utility also decreases for deep space missions as resolution drops with distance. Advanced optical telescopes could have helped confirm Columbia's condition, but they were used too little and too late.[1] Ground-based cameras recorded Columbia during launch, but they lacked the resolution and frame rate required to determine the extent of lost foam and its impact speed at the TPS [Fig. 1(a)].[1]

Spacecraft rendezvous, an option for very few missions, provides excellent inspection resolution and coverage, but the cost and risk can be high, and the response may be slow. Rendezvous with the International Space Station (ISS) would have confirmed Columbia's condition but was not possible due to the additional fuel that would have been required to change Columbia's orbit. After the Columbia incident, all but one of the Space Shuttle Missions launched to the orbit of the ISS, so the ISS crew could image the TPS [Fig. 1(b)]. This constraint prevented the Space Shuttle from visiting other orbits.[7]

EVA inspection, available for piloted missions only, can provide inspection with high resolution, good coverage, and rapid response, but the risk associated with astronaut EVA is significant. EVA could have confirmed Columbia's condition, but it was not performed. After Columbia, whenever TPS damage was identified during ISS rendezvous, astronauts performed EVA to more completely characterize TPS condition.[8]

Robotic arms, designed specifically for inspection, can have very high resolution, rapid response, moderate coverage, and low risk, but this comes with added cost. General-purpose robotic arms repurposed for inspection may not add cost, but they may have limitations in coverage and resolution. The space shuttle's Canadarm robotic arm was used during the 1993 flight of

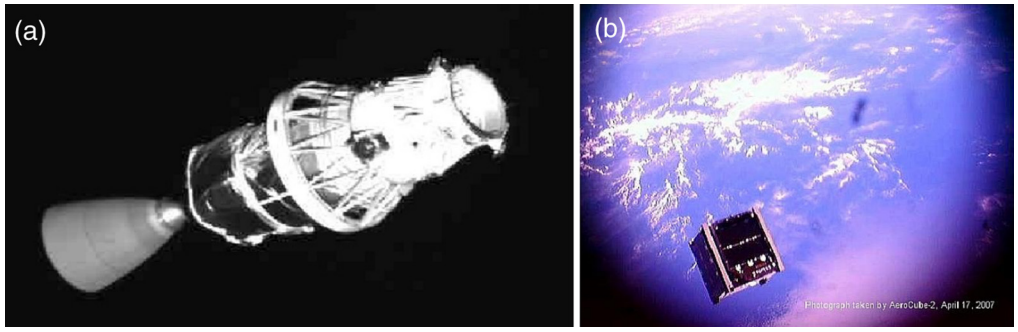

Fig. 2 Examples inspection results from free flyers. (a) Image of the Delta-K upper stage of the Delta-II launch vehicle, captured by the XSS-10 spacecraft. Public domain. Credit: Air Force Research Lab. (b) Image of Cal Poly's CP6 as captured by The Aerospace Corporation's AeroCube-2, which was deployed simultaneously.[17] Reproduced with permission, courtesy of The Aerospace Corporation.

Atlantis to confirm damage to the TPS, but the image quality was inadequate to confirm the extent of the damage. Canadarm was not included on Columbia's 2003 mission.[9] After Columbia, all flights included the Orbiter Boom Sensor System, an extension to Canadarm, which used lidar to scan the TPS.[10]

On-board inspection can provide real-time, high-resolution information with limited coverage at low risk and low cost. On-board inspection may be accomplished by the crew with handheld cameras or autonomously with vehicle-mounted cameras. Footage of Columbia's external tank separation, captured by the crew, may have confirmed the extent of foam loss, but it was not fully requested for review before reentry.[1] Some TPS panels were visible from inside the orbiter, but the affected panels (under the wing) were not, which are evident in Fig. 1(d).

Free-flying inspectors have potential for high-resolution, full-coverage condition estimation. Their response is rapid if stored in the vehicle but may be slow if required to rendezvous from a different orbit. The dynamics of spaceflight and the sensitivity of most spacecraft exteriors make this approach potentially risky or expensive. AERCam Sprint, which demonstrated free-flying, remote-controlled inspection during Columbia's 1997 mission, could have rapidly confirmed Columbia's condition, but it was not included on Columbia's 2003 mission. Since Columbia, several civilian, follow-on inspectors have been proposed,[11,12] but their demonstration has been restricted to the interior of the ISS.[13–15] In 2006, the U.S. Air Force conducted several on-orbit experiments for satellite servicing, including significant demonstrations of inspection performed by an autonomous free-flyer[16] [see Fig. 2(a)]. Most of the results of these experiments are classified.[18]

CubeSats present a unique opportunity for remote inspection, thanks to their low cost and brief, *de facto* proximity to their launch vehicles after deployment. Previous on-orbit tests of remote inspection using a CubeSat yielded mixed results. AeroCube-2 successfully inspected another CubeSat during release [see Fig. 2(b)],[17] but separation rates make inspection of the launch vehicle difficult with a single camera. AeroCube-3 attempted to use a tether with the launch vehicle to maintain extended proximity and camera orientation but was unsuccessful.[19]

2 Passive CubeSat Approach

To demonstrate the viability of using CubeSats to perform remote inspection of space vehicles, we are implementing a passive CubeSat approach. As CubeSats are deployed, they are briefly in proximity with the vehicle that deploys them. Safety standards have made CubeSat deployment a relatively routine, safe operation. The CubeSat standard allows CubeSats to power on immediately after separation from the dispenser, as long as antenna deployment and radio transmissions are inhibited for an additional 30 and 45 min, respectively.

The PIC complies with the CubeSat standard and rapidly boots after release to image the upper stage of its launch vehicle and other satellites being deployed simultaneously. We further minimize inspection risk by not using a tether, attitude control, or propulsion systems. This

ensures that the inspector is passive, with no ability to alter the outward velocity provided by the CubeSat dispenser spring system. Rapid boot is driven by a field-programmable gate array (FPGA). A spherical camera array compensates for any separation tumble by imaging the entire surroundings of the inspector.

Passive inspection CubeSats can be low cost because of the CubeSat standard,[20] launch ride-share, lean development approaches, and increased risk tolerance using electronic components mass-produced for consumer electronic devices.[21] The resolution has the potential to be very good but may be affected if separation tumble is high. The response time can be rapid since an increasing number of spacecraft deploy CubeSats and could easily store one or more CubeSat inspectors for on-call deployment.[22–25] The coverage is limited but may be improved if the target rotates. Each PIC is single-use, so multiple inspections require multiple units. For missions anticipating limited need for inspection, the PIC is a uniquely safe and affordable solution.

3 Passive Inspection CubeSats Demonstration Mission and Technical System Description

We developed the PICs mission to demonstrate the PICs concept. The goal of the mission is to show CubeSats' ability to rapidly boot and image the launch vehicle after deployment without the need for attitude control. We have done this by designing and building two identical 1U CubeSats (PIC-A and PIC-B), which are manifest for a 2019 launch on Virgin Orbit's LauncherOne. Two identical CubeSats were built in order to provide redundancy and a known imaging target. Both units will be deployed simultaneously from the same CubeSat dispenser pod. Immediately after separating from the launch vehicle, the PICs rapidly power on and collect images of their entire surroundings, including the launch vehicle and other satellites being released. In case of low lighting conditions, a flash system illuminates nearby objects. Note that in this configuration, the satellites will be able to inspect only the portion of the launch vehicle visible to them as they drift away. Future missions may involve additional CubeSats to improve inspection coverage. This mission is a first step toward that goal. After these images are fully downlinked, the PICs capture virtual reality images and observe mesoscale atmospheric phenomena, including lightning storms, cloud coverage, and aurorae. The operational activities required to accomplish these objectives are divided into four stages, which are detailed in Table 2.

3.1 *Flight System*

Primary flight system requirements for the PICs demonstration mission include affordability, reliability, resolution, coverage, and response. These require good power retention, rapid boot-up, wide field of view, and fine spatial resolution. Good power retention and rapid boot-up ensure that the flight system is able to begin imaging before drifting away. Wide field

Table 2 Summarized concept of operations (CONOPS) for the PICs mission.

Stage	Objective	Tasks	Duration
I	Inspect parent and sibling vehicles	Rapidly boot, illuminate flashes, and capture images (three sets of six images, 700 kB/image)	1 min
II	Save inspection data	Copy inspection data from cameras to on-board memory, collect telemetry, save telemetry	15 min
III	Downlink inspection data	Collect telemetry, transmit telemetry beacons (every 30 s), downlink images and historical telemetry from satellite to ground (1 pass/day, up to 7.5 MB/pass)	2 to 4 days
IV	Extended mission	Collect telemetry, transmit telemetry beacons, capture remote sensing images and spherical images for educational virtual reality experiences, downlink images and historical telemetry	Until end of life

of view ensures that the launch vehicle is captured in the images. Fine spatial resolution ensures that small elements of the target's condition are visible. In Sec. 4, we evaluate the expected performance of the flight system design with respect to these key performance measures.

The flight system is composed of a mixture of custom and off-the-shelf components, as shown in Fig. 3. An interface diagram for the electrical components is given in Fig. 4. Custom components include a combined electrical power control board and FPGA interface, a spherical array of identical solar harvesters, which also hold the light-emitting diodes (LEDs), and antenna deployment mechanisms, a modular battery system, an ultra-high frequency/very-high frequency (UHF/VHF) radio, a spherical uplink/downlink antenna array,

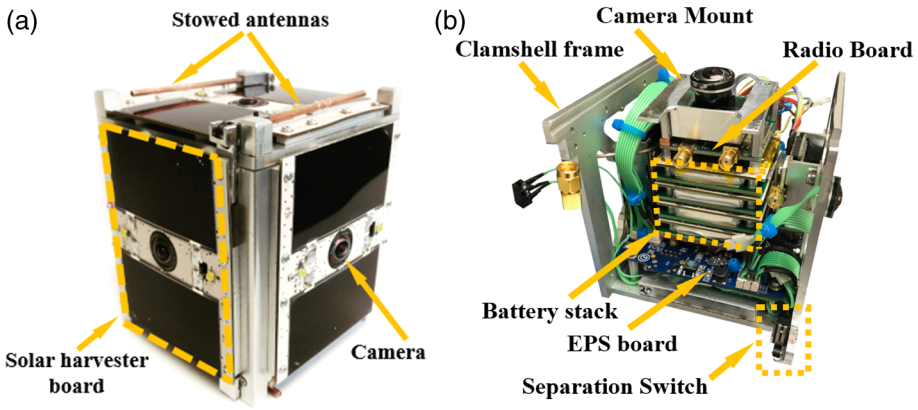

Fig. 3 Photo of the PICs engineering unit. (a) Exterior view of the PICs engineering unit with antennas in stowed position. (b) PIC interior structure, with radio board, battery stack, EPS board, and four cameras attached to one of two clamshells. The clamshells, described in Sec. 3.1.6, comprise the retired chassis design.

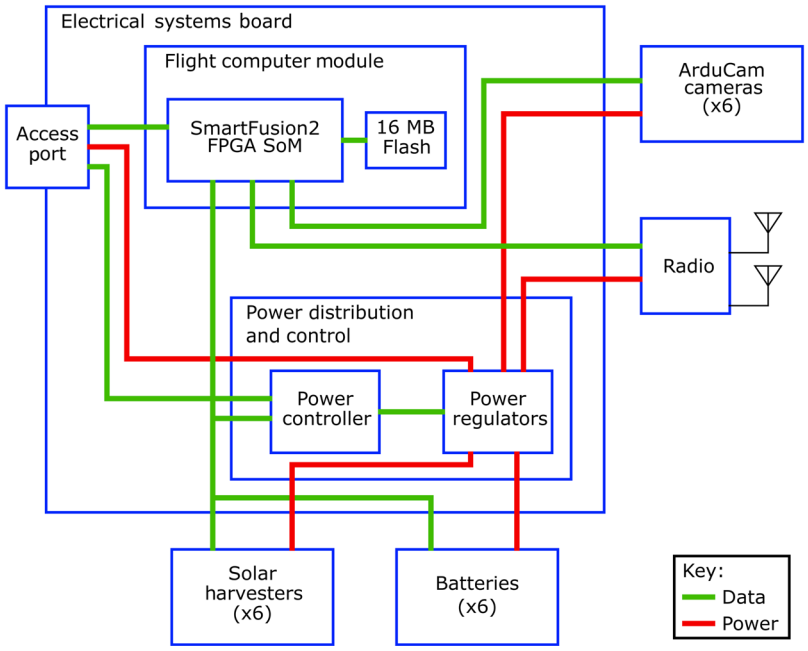

Fig. 4 Block diagram of the PICs electrical systems and their data and power interfaces. The flight computer module interfaces with the cameras, radio board, flash memory, and micro-USB access port. It also communicates with the solar harvester, monitors battery boards, and collects telemetry. The power distribution and control module routes access port charge power to the batteries and routes battery power to the rest of the system. Note the electrical systems board is also called the EPS board.

heatsink brackets for thermal management, camera mounting brackets, and chassis. Off-the-shelf components include ArduCam cameras and a SmartFusion2 FPGA system on module (SoM). These components are introduced in subsequent sections, grouped into the following subsystems: camera, command/data handling, power, communications, thermal, and assembly.

3.1.1 *Camera array*

The main payload for PICs is the camera array, which is composed of six cameras, one on each face of the CubeSat. The camera array is supported by an array of 12 high-power LEDs that illuminate targets during the initial imaging period. Each camera is a board-level ArduCam module consisting of an Omnivision OV5642 5 MP camera sensor, an 8-MB static random-access memory (SRAM) frame buffer, and a low-power complex programmable logic device capture controller. The OV5642 camera sensor captures color images from the visible light spectrum on a 2592×1944 pixel array with a 1/4″ focal plane. It performs on-board discrete cosine transform-based JPEG compression. The image sensor is fitted with a 1.55-mm focal length M12 lens, giving a field of view of 132 deg × 104 deg.

The ArduCam camera module is used primarily because of the limited inputs, outputs, and signaling hardware of the SmartFusion2. ArduCam uses a two-wire I2C configuration bus and a four-wire, serial peripheral interface (SPI) data bus. The configuration bus for all six cameras is tied together, and each camera's SPI bus connects independently to the SmartFusion2 FPGA.

As a lesson learned, we note that allowing constraints of the flight controller to determine camera selection led to a suboptimal choice for the cameras. ArduCam requires use of artifact-prone JPEG compression and restricts image capture to batches of three frames per camera, after which a lengthy data transfer must occur. Selecting camera sensors with parallel data transfer and spending more time developing an FPGA-based compression and data handling system would improve both image quality and image quantity.

3.1.2 *Command and data handling*

The command and data handling (C&DH) subsystem has at its core the SmartFusion2 SoM, which includes an Arm Cortex-M3 processor and FPGA fabric combined into a system on chip (SoC). The C&DH subsystem uses the SoC to control the CubeSat's main operations. The SmartFusion2 consumes little power and uses a flash-based FPGA, which is more reliable in radiation environments than comparable SRAM-based FPGAs. The ARM CPU on the SmartFusion2 runs uCLinux, a version of Linux for devices with no memory management units. The centrality of the SmartFusion2 within the C&DH subsystem can be seen in Fig. 4.

The C&DH subsystem addresses tasks by running individual software processes on top of uCLinux. These software processes control several responsibilities, including image capture, telemetry gathering, response to network commands, and overall system monitoring.

During the first stage of the mission, only the imaging task is active. To initialize it, the SoM processor writes values to registers contained in the SoM FPGA fabric. The six cameras have their own individual SPI buses and each is connected to the FPGA. Once the FPGA is commanded to begin image capture, it simultaneously commands all cameras to capture a burst of three images. Each camera stores its captured images on a small 8-MB SRAM frame buffer. Following image capture, the SoM processor and FPGA then control the transfer of the captured images, transferring the images from the cameras, through the FPGA interface, and out to nonvolatile flash memory. Once the images are safely stored in nonvolatile memory, the cameras can be turned off to conserve power and the images can be transferred to the ground station at a later time.

After initial imaging is complete, additional software tasks are initiated. These tasks execute on repeat for the remainder of the CubeSat's functional life. They autonomously collect and transmit telemetry, monitor the network for commands from the ground station, and monitor other subsystems to maintain system health. When there is a change in the system state, such as a low power level, the system health monitor adjusts the CubeSat's operations to correct the change. Faults are logged and included in telemetry for later review by ground-station operators.

Table 3 Power budget and duty cycle for primary mission operations. See Table 2 for descriptions of stages I to IV.

	Stage I		Stage II		Stage III		Stage IV	
	Power	Duty cycle	Power	Duty cycle	Power	Duty cycle	Power	Duty cycle
On-board processing	8 W	1%	1 W	100%	1 W	100%	1 W	100%
Imaging	8 W	9%	1 W	100%	N/A	N/A	N/A	N/A
Image downlink	N/A	N/A	10 W	4%	4 W	1%	4 W	1%
Power generation	N/A	N/A	+2 W	60%	+2 W	60%	+2 W	60%
Telemetry beacons	N/A	N/A	N/A	N/A	1 W	3%	1 W	3%
Stage duration	1 min		15 min		2 to 4 days		Lifetime	
Net capacity change	**−1%**		**−4%**		**+5%**		**0%**	

Note: The final line is bolded to indicate key summary information.

3.1.3 *Power*

The power subsystem consists of three main segments: power generation (solar cells and solar harvesting circuitry), power storage (battery stack and charging circuitry), and power management [voltage regulation circuitry on the main electrical power system (EPS) board]. The interfaces between these segments and the power they provide to the rest of the electrical system are visible in Fig. 4. The PICs use gallium arsenide solar cells to generate 1 to 2 W of electrical power, depending on the CubeSat's orientation with respect to the Sun. The solar cells are affixed to each face of the CubeSat via solar harvester circuit boards. Current generated in the solar cells is fed through to the battery pack to charge four off-the-shelf LiPo batteries, with a total of 3.5 A-hr power storage capacity. Each battery is sandwiched between a battery charge-controller board and a dedicated heater board. The heater board integrates a trace resistance heater that is used to keep the batteries warm during the eclipsed portion of the orbit. Last, power is managed and distributed by the EPS board, which contains voltage regulators as well as voltage and current sensors to track the power draw of the CubeSat. Power system diagnostic data are included in downlinked telemetry. Specific values for power draw during primary mission operations can be found in Table 3.

3.1.4 *On-board communications*

The on-board communication subsystem provides telemetry, tracking, and command (TT&C) services and downlinks mission data. The compact (5 cm × 5 cm), low-power radio board provides high-efficiency, high-throughput, and full-duplex uplink and downlink capability. Downlink operates at up to 300 Kbps. Uplink operates at up to 115.2 Kbps. The radio employs the Consultative Committee for Space Data Systems (CCSDS), Space Data Link Protocol, and Space Packet Protocol standards for space communications. It operates at 2-W forward power with >50% efficiency. It operates at very low power during receive operations and when idle. In Table 4, the downlink and uplink link budgets can be found, demonstrating that PICs achieve a workable link with acceptable margin. The downlink budget has ∼7.2 dB of link margin, and the uplink budget has ∼10.5 dB of link margin for a 10-W transmit. Since our license is up to 100 W, we have up to 20.5 dB of uplink margin.

Without maneuvering systems, the PICs require omnidirectional antennas for both TT&C and downlink. The antenna system includes a dipole for transmitting and a loaded monopole for receiving. The PICs structural frame and solar harvester boards act as a ground plane. During launch and deployment, the antennas are kept in the stowed position. Once the antenna deployment command is given, 1.6 A of current heats a bare nickel chromium burn wire, which melts

Table 4 Link budget summaries for the PICs mission communications system.

Link element	Unit	Downlink	Uplink
Transmitter[a] (Tx) EIRP	dBW	4.0	27.1
Channel losses	dB	159.4	150.6
Receiver[b] (Rx) isotropic signal level	dBW	−155.4	−123.5
Rx losses	dB	2.8	5.8
Rx antenna gain	dBi	27	2.2
Rx figure of merit (G/T)	dB/K	−2.1	−23.8
Rx S/no	dBHz	70.3	76.7
System desired data rate	kbps	300	150
Data rate expressed in dBHz	dBHz	54.8	51.8
10.5 Eb/no	dB	15.6	24.9
Required Eb/no threshold	dB	8.4	13.4
System link margin	**dB**	**7.2**	**10.5**

Note: The final line is bolded to indicate key summary information.
[a]Tx is spacecraft for downlink, ground station for uplink.
[b]Rx is ground station for downlink, spacecraft for uplink.

a loop of nylon that constrains the spring-loaded antennas. With the nylon loops broken, the antennas are free to spring to the deployed position.[26]

Primary inspection data are 12.6 MB in size. At an average rate of 200 Kbps to allow for variation in link quality and other transmissions to be handled, this can be downlinked in ∼8.4 min. Since we assume that we can achieve maximum throughput for up to 5 min of every pass, this should take no more than two passes and no >2 days to downlink primary inspection data (assuming one high-quality pass per day). The estimate in Table 2 shows a maximum of 4 days to allow for time spent in acquiring the CubeSats TLE and ensuring the CubeSat is in a stable state before commencing downlink.

3.1.5 *Thermal management*

The thermal management subsystem uses both passive and active elements to maintain components within their acceptable temperature ranges. The surface area of the satellite not covered by solar cells is coated with white solder mask with high emissivity ($\epsilon = 0.9$) and low absorptivity ($\alpha = 0.2$), which acts as a radiator. Copper heatsinks epoxied to the radio and EPS increases the thermal mass and, along with aluminum heatsinks on the cameras, provides a conductive path for heat dissipation from those components to the chassis and outer surface. Fault switches on the battery control boards disconnect the batteries when half of the thermistors embedded in the boards read over 45°C and do not reconnect until the temperature falls below that value. The same battery board thermistors also feed a control loop that activates copper trace resistance heaters on the batteries in case of extreme cold. These thermal control measures have been tested in both extreme cold and hot scenarios as well as in vacuum and have proven effective in mitigating thermal risks to the PICs mission.

We modeled the PICs thermal environment using a lumped, transient energy balance considering heating from direct sunlight, albedo, earth radiation, and on-board component energy dissipation, as well as cooling from radiation to deep space.[27] The material properties, surface area, and other values needed for this model were obtained from the computer-aided design model and from knowledge of the materials in the components. We created the model to predict a wide range of possible orbits that lead to the coldest temperature ($\beta = 0$ with the longest

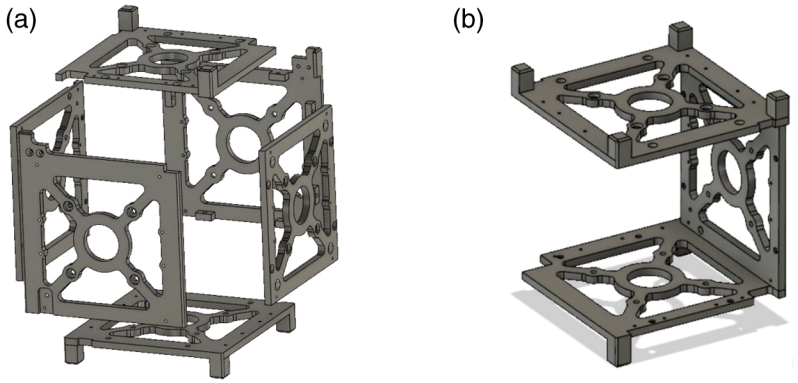

Fig. 5 PICs chassis designs. (a) Final PICs chassis design consisting of six interlocking walls. (b) One of two interlocking segments of the retired PICs chassis design, nicknamed the "clamshell," included as a lesson learned.

satellite eclipse time) and to the hottest temperature ($\beta = 90$ with no satellite eclipse time).[28] The maximum operating temperature of the PICs electrical components was below a 70.6°C peak temperature, enabling the design of a thermal management system, which primarily protects against overheating.

3.1.6 *Assembly*

The PICs assembly system includes the chassis, electronics stack, structural brackets, heat brackets, cables, and fasteners. Elements of this assembly can be seen in Fig. 3(b). The chassis is made up of six interlocking square aluminum walls, which are bolted together to form a cube, as illustrated in Fig. 5(a). Rails and standoffs are integrated into these walls. This chassis design is low cost, easy to produce to tolerance, and easy to assemble and service. Each chassis wall mounts a camera, using an aluminum camera mount, and a solar board, using standoff bars. The solar boards and cameras are electrically connected to the EPS board by custom cables with Molex connectors. These cables are secured to the structure using Tefzel zipties. The electronics stack includes the electrical systems board, four battery sandwiches, and the radio board. Four threaded rods secure the stack to the walls of the chassis.

As another lesson learned, we note the retired design for the PIC chassis, the "clamshell," which is illustrated in Fig. 5(b). The clamshell consists of two U-shaped segments, each of which composed three of the six walls of the CubeSat. While this design is rigid and requires few pieces, its complex production and assembly sequence frequently caused irreparable electrical and tolerance failures and so is not recommended for future spacecraft.

3.2 *Ground Station*

BYU's ground station supports the PICs mission by watching for beacons, receiving and processing downlinked data, and uplinking commands to the CubeSats. It consists of four 10-ft. dishes with interchangeable feeds. Each dish has wide-band low-noise amplifiers and selectable filtering. For the PICs mission transmit antenna, we use a dipole feed at 459 MHz. For the receive antenna, we use an off-the-shelf patch feed at 903 MHz. To acquire the satellites' communication signals when first on orbit, all dishes are fitted with receive feeds to expand the search area. After acquisition, two of these receive feeds are exchanged for transmit feeds.

The processing segment is provided through GNURadio, a Universal Software Radio Peripheral B210 Software-Defined Radio, and a custom software package developed at BYU called Cygnus. It was developed to handle CCSDS specifications and the unique protocols used by PICs. It also operates the four available dishes and multiple channels autonomously. This system provides two receive and two transmit channels with 56 MHz of instantaneous bandwidth.

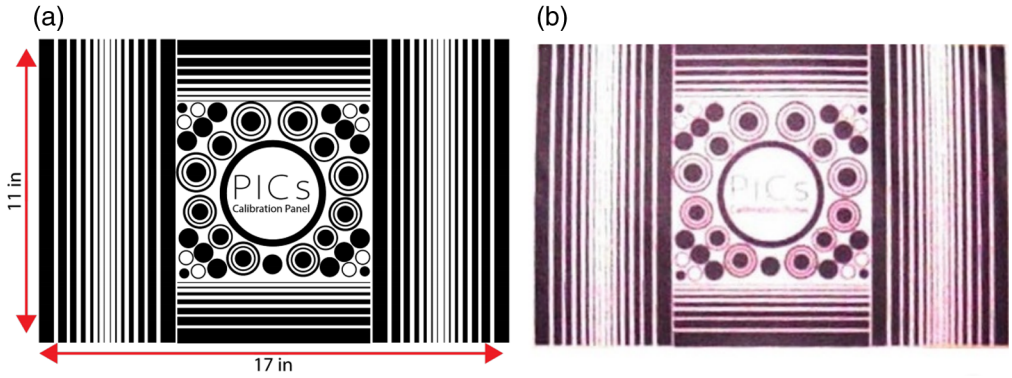

Fig. 6 PIC image test results. (a) The calibration panel used in the PICs imaging test. (b) The image captured by the PICs test unit at a distance of 2 m. Image cropped to include panel only.

4 Expected Performance of the Passive Inspection CubeSats Mission

As discussed in Sec. 3.1, the PICs spacecraft must have good power retention, rapid boot-up, wide field of view, and fine spatial resolution. We proceed to describe expected performance of PICs in each of these categories, based on current tests and models.

Power retention is expected to support more than a year of storage. A composite, 3-month storage test on the PICs engineering unit resulted in a power loss of about 45 mW-h/month. A low-power boot-up test determined that the minimum battery capacity required to complete all primary mission functions was 3.7 V, equivalent to ~40% battery charge. This means primary mission functions will be well powered upon deployment, even after a year delay in launch.

The boot time of the PICs spacecraft is ~1.1 s, tested by timing the CPU. Expected deployment speeds vary from 0.5 to 2 m/s, so we expect the distance from the launch vehicle to be between 0.55 and 2.2 m when the first image is taken.

The field of view is expected to be fully spherical. The wide-angle lenses selected for PICs have a field of view of 132 deg × 104 deg, resulting in complete visibility of the surroundings at the expected imaging distance. We expect the PICs spacecraft to capture images containing the launch vehicle, regardless of deployment tumble.

The spatial resolution of PICs is expected to be roughly 1 mm at a distance of 1 m. To simulate the lighting environment in space, we tested the imaging system in a large room with black walls and a single floodlight. We captured a single stationary image of the calibration panel given in Fig. 6(a) from 2 m away. The result is given in Fig. 6(b). The red tint in the test image is a result of camera settings optimized for low lighting conditions. All circles with a minimum diameter of 1 mm are visible in the captured image. All horizontal lines, with the exception of the 0.75-mm lines, are also distinguishable.

5 Future Work

We predict it will be possible to improve the cost and performance of future PICs demonstrations by making modifications to the mission. Much of the cost of CubeSat design and development stems from the difficulty of designing an electronic system for continued operation in space. By integrating the receiver into the parent spacecraft rather than requiring the CubeSat transmit the data to the ground, the CubeSat could immediately relay data back to the parent spacecraft. This could shorten the required functional life to <30 min, which would reduce cost and size. In addition, use of a weaker dispenser spring could extend proximity by slowing CubeSat separation.

Further missions can be explored. For example, a follow-on inspection CubeSat with attitude control could support additional, directional sensors. With propulsion, the inspector could rendezvous with a variety of inspection targets and maneuver about them to expand coverage for an extended period. Such future work could provide valuable state information for complex space vehicles. Ultimately, the best solution to space vehicle inspection may involve a CubeSat that

separates from its parent vehicle, performs inspection of multiple locations, and redocks with the parent vehicle to recharge and refuel. This solution may provide the best combination of resolution, coverage, and rapid response at acceptable risk and cost. Such a solution may be uniquely suited to inspect space vehicles for ambitious missions in difficult, complex, or unknown space environments.

6 Conclusion

Both remote inspection and on-board instrumentation are necessary to fully estimate the spacecraft condition. Many methods of remote spacecraft inspection exist, including the use of telescopes, spacecraft rendezvous, on-board robotic arms, and free-flying inspectors. However, the use of these methods is limited due to high costs, poor coverage, low resolution, or proximity risks. CubeSats are typically low cost and are in close proximity for high-resolution visual inspection when passively deployed from the launch vehicle in the standard manner. These conditions help make PICs an effective solution for remote inspection of spacecraft in flight. The PICs mission, developed by undergraduate students attending BYU, is expected to demonstrate that PICs can reliably and affordably inspect spacecraft.

Acknowledgments

The research reported in this article was funded by the NASA Undergraduate Student Instrument Program (NASA Grant No. NNX16AI69A) and the National Science Foundation (Grant No. 1749395). The authors gratefully acknowledge additional support from L3 Technologies and the Fulton College of Engineering at Brigham Young University. Further thanks go to the many undergraduate students involved in the project, including Andrew Orme, Troy Hinckley, Tyler Peterson, Nick Walton, Daniel Fussell, Luke Newmeyer, Christine Akagi, Valerie Fischer, Riley Creer, Zach Brock, Brittany Wilson, Ben Biggs, Dan Merrell, Dan Dahl, Stephen Kimball, Jeff Nybo, Mark Oman, Connor Olsen, Alexis Fisher, Connor Weeks, Evan Jones, Andrew Okazaki, David Strobehn, Michelle Crowder, Chloe Roedel, Keith Garfield, Kevin Shelby, Carlos Vilorio, Joseph Quist, Nick Duehring, Logan Meyer, Stephen Hills, Blake Goodfellow, Mark Moomey, Wes Rogers, Hailey Bischoff, Caleb Smith, Andy Marble, Brandon Snow, Anna Larson, Levi Powell, Jared Ryan, Ben Francis, and Jacob Stratford.

References

1. Columbia Accident Investigation Board, *Report of the Space Shuttle Columbia Accident Investigation*, National Aeronautics and Space Administration, Washington, D.C. (2003).
2. E. M. Jones, "One small step," *Apollo 11 Lunar Surface Journal, National Aeronautics and Space Administration*, 1995, https://www.hq.nasa.gov/alsj/a11/a11.step.html (Accessed 26 March 2019).
3. K. Edgett et al., "Curiosity's Mars hand lens imager (MAHLI): Sol 0–179 activities, observations, range and scale characterization," in *Eur. Planet. Sci. Congr.*, Vol. 8, p. EPSC2013–246 (2013).
4. R. Ridenoure, "RocketCam systems for providing situational awareness on rockets, spacecraft, and other remote platforms," *Proc. SPIE* **5418**, 94–104 (2004).
5. S. K. Krikalev, "ISS011-E-11263," *International Space Station Imagery, Spaceflight Gallery, National Aeronautics and Space Administration*, 2005, https://spaceflight.nasa.gov/gallery/images/station/crew-11/html/iss011e11263.html (Accessed 26 March 2019).
6. NASA/JPL-Caltech/MSSS, "Routine inspection of rover wheel wear and tear," *Mars Exploration Program and Jet Propulsion Laboratory, National Aeronautics and Space Administration*, 2016, https://mars.nasa.gov/resources/routine-inspection-of-rover-wheel-wear-and-tear/ (Accessed 26 March 2019).
7. *Space Shuttle Mission STS-134 Final Flight of Endeavor Press Kit*, National Aeronautics and Space Administration (2011).

8. A. Heiney, "Mission STS-118: Investing in future exploration." *Kennedy Space Center, National Aeronautics and Space Administration*, 2007, https://www.nasa.gov/mission_pages/shuttle/behindscenes/sts118_overview.html (Accessed 26 March 2019).
9. J. W. Thomas, "STS-27R OV-104 orbiter TPS damage review team summary report," Technical Report NASA-TM-100355-VOL-1, NAS 1.15:100355-VOL-1, National Aeronautics and Space Administration (1989).
10. R. O. Nellums et al., "3D scannerless LADAR for orbiter inspection," *Proc. SPIE* **6220**, 62200G (2006).
11. S. E. Fredrickson et al., "Application of the Mini AERCam free flyer for orbital inspection," *Proc. SPIE* **5419**, 26–35 (2004).
12. C. Henshaw, L. Healy, and S. Roderick, "LIIVe: a small, low-cost autonomous inspection vehicle," in *AIAA SPACE 2009 Conf. & Exposition* (2009).
13. S. B. McCamish et al., "Flight testing of multiple-spacecraft control on spheres during close-proximity operations," *J. Spacecraft Rockets* **46**(6), 1202–1213 (2009).
14. D. Fourie et al., "Flight results of vision-based navigation for autonomous spacecraft inspection of unknown objects," *J. Spacecraft Rockets* **51**(6), 2016–2026 (2014).
15. D. Sternberg et al., "Reconfigurable ground and flight testing facility for robotic servicing, capture, and assembly," in *IEEE Aerosp. Conf.*, IEEE, pp. 1–13 (2016).
16. M. Osborn et al., "Micro-satellite technology experiment (MiTEx) upper stage propulsion system development," in *43rd AIAA/ASME/SAE/ASEE Joint Propul. Conf. & Exhibit*, p. 5434 (2007).
17. A. Chin et al., "CubeSat: the pico-satellite standard for research and education," in *AIAA Space 2008 Conf. & Exposition*, p. 7734 (2008).
18. D. Barnhart et al., "Xss-10 micro-satellite demonstration," in *AIAA Defense and Civil Space Programs Conf. and Exhibit*, p. 5298 (1998).
19. H. J. Kramer, "Aerocube-3," *Earth Observation Portal Directory, European Space Agency*, https://directory.eoportal.org/web/eoportal/satellite-missions/a/aerocube-3 (Accessed 31 March 2019).
20. J. Puig-Suari et al., "CubeSat Design Specification (CDS), Rev. 13," *The CubeSat Program*, Cal Poly SLO, https://static1.squarespace.com/static/5418c831e4b0fa4ecac1bacd/t/56e9b62337013b6c063a655a/1458157095454/cds_rev13_final2.pdf (2 February 2014).
21. C. Boshuizen et al., "Results from the Planet Labs flock constellation," in *Proc. AIAA/USU Conf. Small Satellites*, American Institute of Aeronautics and Astronautics (AIAA), Vol. 28 (2014).
22. R. Pournelle and M. Johnson, "Nanoracks CubeSat deployment services," in *AIAA/USU SmallSat Conf., Pre-conf. CubeSat Developers' Workshop* (2014).
23. D. Hitt, K. F. Robinson, and S. D. Creech, "NASA's Space Launch System: a new opportunity for CubeSats," in *5th Interplanet. CubeSat Workshop, Technol. Session* (2016).
24. K. R. Fisher, "Utilizing the deep space gateway as a platform for deploying CubeSats into lunar orbit," in *Deep Space Gateway Science Workshop 2018*, USRA, NASA Johnson Space Center, Houston, Texas (2018).
25. W. Frick and C. Niederstrasser, "Small launch vehicles—a 2018 state of the industry survey," in *Proc. AIAA/USU Conf. Small Satellites, Session 9: Space Access (306)*, 2018 https://digitalcommons.usu.edu/smallsat/2018/all2018/306/.
26. A. Thurn et al., "A nichrome burn wire release mechanism for CubeSats," in *41st Aerosp. Mech. Symp.*, pp. 479–488 (2012).
27. S. Czernik, "Design of the thermal control system for Compass-1," PhD thesis, Department of Aerospace Engineering, University of Applied Sciences Aachen, Germany (2008).
28. K. Aaron et al., *Spacecraft Thermal Control Handbook, Volume 1: Fundamental Technologies*, The Aerospace Press, El Segundo (2002).

Patrick Walton is the founder of Care Weather Technologies, which develops CubeSats for weather remote sensing. He is concurrently pursuing his MS degree in electrical and computer engineering at Brigham Young University (BYU), Utah. He received his BS degree in mechanical engineering with university honors from BYU in 2017. As an undergraduate student, he was the system engineer and project lead for BYU's Passive Inspection CubeSats mission.

Josh Cannon is pursuing his BS degree in mechanical engineering with minors in computer science and astronomy at BYU. Currently, he is the project lead and head assembly engineer for the PICs mission and plans to continue to pursue spacecraft technology engineering as a graduate student upon completion of his undergraduate degree in December 2019.

Brian Damitz is pursuing his BS degree in mechanical engineering with minors in computer science and aerospace studies at BYU and will graduate in April 2022. He assisted with the development of kernel- and user-space software for BYU's Passive Inspection CubeSat mission.

Tyler Downs is a radar system verification engineer at IMSAR, where he facilitates the testing and bring up of production and prototype radar systems. He graduated in 2018 with a BS degree in computer engineering from BYU, where he worked as the power subsystem lead on the PICs project. He is an avid guitarist and songwriter, performing often at events in the Utah Valley area.

Dallon Glick is a master's student at BYU and is a member of BYU's Configurable Computing Lab. His research interests center around configurable computing and embedded systems. Currently, his research focuses on computer-aided design tools and frameworks for field-programmable gate arrays (FPGAs), such as RapidSmith2, and new FPGA usage models these tools can enable.

Jacob Holtom received his BS degree in electrical engineering from BYU in 2019 and is now pursuing his PhD in electrical engineering. He was the communications lead for BYU's Passive Inspection CubeSats mission. With Dr. Doran Wilde, he designed a 5-cm-square, low-power, full-duplex, 1U CubeSat radio that supports experimental spread spectrum modulation at speeds up to 300 kbps. He previously worked at L3 Technologies on communications and radar systems.

Nicholas Kohls received his BS degree in computer engineering in 2019 from BYU. He worked as an undergraduate student developing the electric power system for BYU's Passive Inspection CubeSat. Currently, he is a master's student at BYU doing research under Dr. Long on digital beamforming.

Alex Laraway is a career machinist pursuing his BS degree in manufacturing engineering at BYU. As the lead manufacturing engineer for BYU's Passive Inspection CubeSats mission, he fabricated most of the mechanical hardware. His primary research interest is in affordable space technology through concurrent design, lean manufacturing, and rapid prototyping.

Iggy Matheson obtained his BS degree in mechanical engineering from BYU in 2016 and will obtain an MS degree in aerospace engineering from Utah State University in 2019. A PhD from the University of Arizona is expected to follow by 2023. His research interests revolve around orbital mechanics. Prior recognitions include a summer research fellowship administered by Southwest Research Institute and an NSF graduate research fellowship.

Jason Redding is pursuing his BS degree in mechanical engineering at BYU with expected completion in 2021. His interest in small spacecraft and their applications led him to be a part of BYU's Passive Inspection CubeSats mission, where he is the test engineering lead.

Cory Robinson received his BS degree in mechanical engineering from BYU in 2017. As an undergraduate student he led the mechanical team for BYU's Passive Inspection CubeSat project and focused his work on the thermal control design. Currently, he lives and works in Northern Virginia.

Jared Ryan is pursuing his BS degree in electrical engineering at BYU with expected completion in 2021. He has assisted multiple teams on the Passive Inspection CubeSat project, including the software, assembly, and testing teams. He plans on continuing work with future BYU spacecraft missions.

Niall Stoddard is currently pursuing his BS degree in electrical engineering at BYU. As lead power systems engineer for the Passive Inspection CubeSat at BYU, he finalized the power

design for the last revisions and assisted with the final preparation on the flight units. He expects to graduate in April 2021 and intends to continue in the field of small spacecraft.

Jacob Willis graduated with a BS degree in computer engineering from BYU in April 2019. As an undergraduate student, he led the flight software team for BYU's Passive Inspection CubeSats project. He is now pursuing his MS degree in electrical engineering from BYU, emphasizing in guidance, navigation, and control.

Karl Warnick received his BS degree in electrical engineering and mathematics and his PhD in electrical engineering from BYU in 1994 and 1997, respectively. Since 2000, he has been a faculty member in the Department of Electrical and Computer Engineering at BYU. He has published many articles and books on electromagnetic theory, numerical methods, antenna applications, and high-sensitivity phased arrays for satellite communications and radio astronomy.

Michael Wirthlin is currently a professor in the Department of Electrical and Computer Engineering at BYU. He has been actively involved in FPGA design for over 30 years and is active in the FPGA design, architecture, and research communities. His research interests include reliable FPGA design, fault tolerant computing, and configurable computing systems. He has led the development of a number of tools and techniques for improving the reliability of FPGA designs.

Doran Wilde is an emeritus professor in the Department of Electrical and Computer Engineering at BYU, where he taught a wide range of engineering courses, including electric circuit design, integrated circuit design, embedded system design, and computer architecture. He has been actively engaged in research in the fields of computer arithmetic, application specific systems and architectures, and embedded systems. For this project, he led the student team that designed and built the PCBs for the satellite's electrical power system.

Brian D. Iverson is an associate professor at BYU and received his NSF CAREER Award in 2018 for his work in radiative cooling. He has also worked as a senior member of the technical staff at Sandia National Laboratories. His current research efforts include heat and mass transfer topics that exploit high aspect ratio architectures to enhance or control thermal radiation, condensation, and chemical/biological sensing.

David Long worked at NASA's Jet Propulsion Laboratory (JPL) on advanced radar remote sensing systems and scatterometer projects. He is a professor in the Electrical and Computer Engineering Department at BYU, where he teaches upper division and graduate courses in communications, microwave remote sensing, radar, and signal processing. He is the director of the BYU Center for Remote Sensing. He has over 400 publications in signal processing, radar scatterometry, and synthetic aperture radar.